Modeling of Materials for Naval SONAR, Pollution Control and Nonvolatile Memory Application

Joseph W. Bennett, Ilya Grinberg, Young-Han Shin, and Andrew M. Rappe
The Makineni Theoretical Laboratories, Department of Chemistry, University of Pennsylvania, Philadelphia, PA
{bennett4, ilya2, rappe}@sas.upenn.edu and yhshin@postech.ac.kr

1. Introduction

Perovskite oxides of formula ABO_3 have a wide range of structural, electrical and mechanical properties, making them vital materials for many applications, such as catalysis, ultrasound machines and communication devices. Perovskite solid solutions with high piezoelectric response, such as ferroelectrics, are of particular interest as they can be employed as sensors in SONAR devices. When such a material is deformed by underwater sound vibrations, it generates an electric field which can then be interpreted by a computer to gain information about depth and distance. This information is crucial for the defense and operation of naval submarines and vessels. Ferroelectric materials are unique in that their chemical and electrical properties can be non-invasively and reversibly changed, by switching the bulk polarization. This makes ferroelectrics useful for applications in nonvolatile random access memory (NVRAM) devices.

Perovskite solid solutions with a lower piezoelectric response than ferroelectrics are important for communication technology, as they function well as electroceramic capacitors. Also of interest to the Navy is how these materials act as a component in a solid oxide fuel cell, as they can function as a quiet and efficient source of energy. Altering the chemical composition of these solid oxide materials offers an opportunity to change the desired properties of the final ceramic, adding a degree of flexibility that is advantageous for either communications or fuel production needs.

Most of these materials are complex systems with some degree of disorder, making them challenging to study experimentally. However, as it is their complexity which gives them their favorable properties, highly accurate modeling which captures the essential features of the disordered structure is necessary to explain the behavior of current materials and predict favorable compositions for new materials.

Methodological improvements and faster computer speeds have made first-principles and atomistic calculations a viable tool for understanding these complex systems. Offering a combination of accuracy and computational speed, the density functional theory (DFT) approach[1,2] can reveal details about the microscopic structure and interactions of complex systems[3–5]. Information from DFT calculations can also be used to create accurate, yet computationally inexpensive atomistic models for use in molecular dynamics (MD) simulations. Here, we report on our recent studies of density functional simulations of relaxor ferroelectrics[6] and dielectrics containing defects whose tailorable properties are catalytic in nature[7,8] and could be employed in a fuel cell. We also use a combination of bond-valence model and atomistic molecular dynamics simulations to investigate both the order-disorder character and elastic character in ferroelectric materials.

2. Methodology

All of our calculations are performed with our in-house code using the standard local density approximation (LDA)[9] exchange-correlation functional and a plane-wave basis set. This is a complete basis set that offers the advantage of carrying out operations in both real and reciprocal space through fast Fourier transforms. To reduce the computational cost of the calculations, we use designed non-local[10] optimized[11] pseudopotentials to represent the interactions of the nucleus and the core electrons with the valence electrons. Minimization of the energy with respect to the electronic degrees of freedom is done using the blocked-Davidson[12] iterative diagonalization proceedure[13] with Pulay density mixing[14]. Ionic minimization is performed using a quasi-Newton algorithm.[15] DFT calculations are performed on supercells of up to 60 atoms, with a variety of atomic configurations examined to ensure accurate modeling of the disordered perovskite structures.

978-0-7695-3515-9/08 $25.00 © 2008 IEEE
DOI 10.1109/DoD.HPCMP.UGC.2008.77

Molecular dynamics simulations of the domain wall motion in $PbTiO_3$ were performed using an atomistic model. This model is based on electrostatic, repulsive and bonding interactions as encapsulated in Brown's valence theory of bonding in solids.[16] A database of first-principles structures, energies and forces was used to fit the model parameters. Our model proved successful in studies of bulk $PbTiO_3$, providing a firm foundation for studies of domain wall dynamics. In all MD simulations, we used the Nose-Hoover thermostat with 1 fs time step.

3. Results

A. Structure and Stabilization of O-Vacancies

Recent studies of the catalytic conversion of CO to CO_2 using $LaFe_{0.57}Co_{0.38}Pd_{0.05}O_3$ solid oxide perovskite have shown that cationic Pd can be stored within the oxide. Then, under reducing conditions, Pd is extruded from the oxide as fcc-Pd.[17,18] This forms a Pd surface species that is used for CO oxidation, and after the reaction, an oxidizing atmosphere is applied to return the Pd back into the lattice as a cation. This is a cyclable process, preserves the Pd for many uses, and is a more cost-effective catalyst when compared to conventional Pd supported oxides.

To improve upon this concept and find new oxide functionalities directly related to fuel cells, we explored another material, $Ba(Ce_{1-x}Pd_x)O_{3-\delta}$[7,8] (BCP). Ba and Ce were chosen to increase the overall size of the perovskite host, to assist in the mass transport of Pd. Experimentally, compositions of up to x=0.10 were synthesized and characterized, however many questions about the local structure of the cationic Pd and the role of O vacancies remained. Using DFT, we found that doping $BaCeO_3$ with cationic Pd reduces the symmetry of the unit cell from *Pnma* to the space group *P*1. The tilt system in $BaCeO_3$ is severely interrupted with the addition of one Pd. This perturbation breaks the symmetry, distorting the Ce-O bond lengths. The six nearest Ce neighbors all have two distinct sets of Ce-O bond lengths; four bonds around 2.21 Å and two long bonds around 2.36 Å. The second nearest neighbors have six similar bond lengths of 2.28 Å on average. The nearest Ce neighbors to Pd are enclosed within octahedra that distort, then tilt. The distorted Ce octahedra are the result of the formation of strong, short bonds (≈ 2.03 Å) between O and the small Pd^{4+} cation. The bond lengths of 2.03 Å are typical of Pd^{4+} in an O_6 environment.

Of the two BCP structures (shown in Figures 1 and 2) with an oxygen vacancy, the higher energy structure is Structure 2, where the O vacancy is in between two Ce. This is 0.95 eV higher in energy than Structure 1, because the reduction of Pd^{4+} to Pd^{2+} is more favorable than the reduction of two Ce^{4+}. The vacancy in Structure 1 is further stabilized by the formation of a square planar environment around Pd^{2+}. As shown in Figure 1, the Pd in Structure 1 is four-coordinate square-planar, and not five-coordinate square-pyramidal. This is supported by the Pd-O bond lengths in Structure 1. The first four shortest bond lengths are on average 2.04 Å, and the fifth is 2.66 Å. This longer bond length occurs as a result of the apical O in the CeO_5 square pyramid moving away from the Pd. This does not occur in Structure 2, where the vacancy is in between two Ce (Figure 2). All six Pd-O bond lengths in Structure 2 are around 2.02 Å, whereas the two CeO_5 surrounding the vacancy seem to contract inward, as seen from the bond lengths. These bond lengths are similar to those seen in the structure where there is no vacancy.

This clearly indicates that Pd reduction via an O vacancy may be needed to alleviate some of the strain of this system induced by the small Pd^{4+} ion. When an O vacancy is placed between two Ce, as in Structure 2, the closest corner sharing octahedra decrease their tilt angles to either 9 or 2°. The average tilt angle in Structure 2 is 9.9±5.1°. In Structure 1, when the vacancy is between Pd and Ce, the corner sharing octahedra are not as affected, decreasing their tilt angles by at most 2°. The average tilt angle of Structure 1 is 9.9±3.4°. The average tilt angle of Structures 1 and 2 is the same, but the standard deviation is larger for Structure 2. The largest interruption of concerted tilt systems by a vacancy occurs in Structure 2, where it is not stabilized by the Pd^{2+} cation. All supercell structures resemble the tilt system $a^-a^+a^-$, however, symmetry has been broken by both the Pd substitution and accompanying O vacancy.

To elucidate the local structure of a disordered perovskite, such as BCP, we simulate a neutron-scattering pair distribution function (PDF) by combining DFT-computed atomic positions and known neutron scattering factors. To make direct comparison with experimental neutron PDF, we subtract the average number density and multiply by $4\pi r$:

$$G(r) = 4\pi r\left(\rho(r) - \rho_0(r)\right) \quad (1)$$

where $\rho(r)$ is the microscopic pair density and $\rho_0(r)$ is the average number density. The experimental PDF $G(r)$ of BCP generated with the program PDFFIT[19] matches closely the DFT-derived PDF of Structure 1 generated by an in-house code used in previous studies[20,21]. The correspondence in peaks, as shown in Figure 3, is strong, especially for short r. This further supports the agreement between experimental data and our calculations, as well as the assignment of Pd^{2+} being stabilized by an O vacancy in Structure 1. This provides further evidence that Pd-vacancy pairs are present in the experimentally prepared BCP sample.

The experimentally as-prepared sample that contained cationic Pd had a higher activity than the reduced material, and this activity was similar for Pd-dopant levels 5 and 10%.[8] Different between the two dopant levels was their ability to enhance oxygen mobility through the perovskite lattice at low temperatures. The higher concentration of Pd led to a higher concentration of O vacancies, so O diffusion through the bulk to the surface increased relative to the lower concentration of Pd.

B. Relationship Between Local Structure and Relaxor Behavior

One of the most intriguing properties of relaxors is their temperature-and frequency-dependent dielectric response. While normal ferroelectrics exhibit a narrow peak in dielectric constant versus temperature around the ferroelectric phase transition T_c, relaxors show a broad peak with a full width at half max of 50K or more (suggesting a "relaxed" transition). Furthermore, the dielectric response and in particular the temperature $T_{\epsilon,max}(\omega)$ which maximizes the dielectric constant depends strongly on frequency ω. While several attempts have been made to relate perovskite relaxor properties to the material composition, these have not been successful, due to limited knowledge of B-cation arrangement and the lack of accurate information about the local structure. We show that once these obstacles are eliminated (by recent synthesis of Pb-based relaxor perovskites with long-range B-cation ordering and by the availability of local structural information from DFT calculations), the extent of relaxor behavior can be predicted from the crystal chemical properties of the constituent ions.

To understand the origins of the unusually large dispersion in $Pb(Sc_{2/3}W_{1/3})O_3$-$PbTiO_3$ (PSW-PT) solutions, we search for correlations between the experimentally observed ΔT_{disp} values and crystal chemical parameters such as ionic valence and ionic displacement. Recent theoretical and experimental research showed that the changes in the local potential energy surface of the Pb cations are responsible for compositional phase transitions in Pb-based systems.[3,22,23] Pb off-centering, which gives rise to ferroelectricity in $PbTiO_3$ and derived materials, is due to the energetically favorable formation of short Pb-O bonds.[24] For oxygen atoms with high valence B-cation neighbors (e.g., two Nb atoms in $Pb(Mg_{1/3}Nb_{2/3})O_3$) such short bonds would lead to oxygen bond order greater than two. This violation of oxygen bond order conservation is unfavorable.[22,25] Similarly, oxygen atoms with two low-valence B-cation neighbors (e.g., two Sc atoms in $Pb(Sc_{2/3}W_{1/3})O_3$) would strongly favor Pb displacement in their direction. This gives rise to variations in the local potential, corresponding to the variation in the value of the h parameter in spin models, which disrupts ferroelectricity and gives rise to the relaxor phase[26].

As a measure of the degree of local potential fluctuations, we use the second moment of the valence of the two B-cation nearest neighbors of each oxygen atom ($\langle V^2 \rangle$), defined as

$$\left\langle V^2 \right\rangle = \frac{1}{N_{\mathrm{O}}} \sum_i \left(V_{i,1}^B + V_{i,2}^B - 2\overline{V^B} \right)^2 \qquad (2)$$

where the i index runs over all of the O atoms and $V_{i,1}$ and $V_{i,2}$ are the valences of the two nearest B-cation neighbors of the ith O atom. The first moment of the oxygen atom B-cation neighbor valence $\overline{V^B}$ is equal to four in all Pb-based perovskites.

The other relevant crystal chemical parameter is the average B-cation displacement away from the high-symmetry cubic structure. Our recent research has underscored the importance of cation displacements for compositional phase transitions among the different ferroelectric phases as well as for relaxor-to-ferroelectric transitions[22,23]. Larger B-cation off-center displacements allow the overbonding (underbonding) of oxygen atoms to be alleviated by motion of the B-cations away from (toward) the O atom, tending to stabilize normal ferroelectric phases relative to relaxor or other disordered phases.

To study correlations between local atomic structure and dielectric dispersion, we develop and test our model for all 21 Pb-based relaxor perovskite systems[27–31] for which both the local cation order and the dielectric response have been determined experimentally, including all ordered and some disordered systems.

To obtain average values of B-cation displacements for these systems, we perform DFT calculations using the LDA and 40- and 60-atom supercells.

Combining the two crystal chemical parameters, we propose a simple linear relationship between $D_{\mathrm{B,avg}}$,$\langle V^2 \rangle$ and ΔT_{disp}, such that

$$\Delta T_{\mathrm{disp}} = a_V \left\langle V^2 \right\rangle - a_D D_{\mathrm{B,avg}} + C, \qquad (3)$$

where a_V , a_D, and C are constants. The ΔT_{disp} predicted by the fit a_V , a_D, and C (13K, 438 K/Å, 56.5K respectively) are in good agreement with the observed ΔT_{disp} values, shown in Figure 4.

We can also characterize the compositional relaxor to ferroelectric transition with a Landau theory free energy expression

$$G = G_0 - \frac{1}{2} A\left(\left\langle V^2 \right\rangle, D_{\mathrm{B,avg}} \right) \Delta T_{\mathrm{disp}}^2 + \frac{1}{4} \Delta T_{\mathrm{disp}}^4, \qquad (4)$$

$$\Delta T_{\mathrm{disp,equil}}^2 = A\left(\left\langle V^2 \right\rangle, D_{\mathrm{B,avg}} \right) \qquad (5)$$

$$A\left(\left\langle V^2\right\rangle, D_{\mathrm{B,avg}}\right) = a_0 + a_v\left\langle V^2\right\rangle + a_d e^{-kD_{\mathrm{B,avg}}} \quad (6)$$

where G is the free energy of the relaxor phase, G_0 is the energy of the parent ferroelectric phase and the Landau coefficient A is a function of $\langle V^2\rangle$ and $D_{\mathrm{B,avg}}$(a_0, a_v , a_d, and k are constants).

We have shown that the relaxor or ferroelectric behavior of lead perovskite systems can be predicted by simple Landau theory, where the crystal chemical parameters $D_{\mathrm{B,avg}}$ and $\langle V^2\rangle$ change the magnitude of the second order Landau coefficient. More importantly, the extent of the dielectric dispersion and the strength of the relaxor phase can be quantitatively predicted as well.

C. Multiscale Approach for Understanding Ferroelectric Properties: Phase Transition Characteristic and Domain Dynamics

Ferroelectric materials have been widely studied in both experimental and theoretical investigations due to their applications such as Naval SONAR and non-volatile memories.[32] When an electric field is applied to ferroelectric materials, the polarization direction changes toward the field direction. This state remains after the field is turned off. In studies of the field dependence of ferroelectrics by Merz, Miller and Weinreich, and Stadler[33–35], it was found that the nucleation rates at domain walls have an exponential relation to the external electric fields. Since the speed of non-volatile memory is related to the speed of domain wall motion, there have been many experiments studying domain dynamics.[36–38]

For the theoretical understanding of ferroelectric domain dynamics, we developed a multiscale approach based on first-principles calculations, which was successfully applied to lead titanate ($PbTiO_3$).[39–41] Since $PbTiO_3$ has a perovskite crystal structure with a simple tetragonal-to-cubic phase transition at 765K, it can be a prototype material to understand ferroelectric properties, such as the phase transition characteristics and the ferroelectric domain dynamics. We made a model potential for $PbTiO_3$ by using the relation between bond length and bond valence with sum rule for each atom[16], and the potential parameters were fitted to the DFT calculations.

Using the potential model[39], the mechanism of the ferroelectric domain wall motion was studied in the atomistic molecular dynamics (MD) simulations[40]. MD results show that the formation probability of oppositely polarized critical nuclei on the 180° ferroelectric domain wall is following the Poisson distribution as a limit of the binomial distribution, and nucleation rates are obtained from fitting MD results to the Poisson distribution. As shown in Figure 5, the size of the critical nucleus is 12×12 Å^2, which is much smaller than predicted by Miller and Weinreich's (MW) model of ferroelectric domain wall motion.[34] In order to correct the MW model, we suggested that the boundary of the critical nucleus is diffuse, as demonstrated by the MD results in Figure 5. This diffuse boundary model based on the Landau-Ginzburg-Devonshire theory gave good agreement with MD simulations in the critical nucleus as well as the diffuseness of the critical nucleus boundary, and the activation field obtained from the diffuse model agreed well with MD simulations and experiments.

Since the computed phase transition temperature of $PbTiO_3$ is lower than the experimental value by 200K, we tried to improve the potential parameters without changing the structure of the model potential. When the model with the original parameter set[39] was applied to strained states, the energy difference between DFT and model calculations for $\mathbf{T}^{(11)}$, $\mathbf{T}^{(13)}$, and $\mathbf{T}^{(33)}$ strain tensor elements is very large (Figure 6(a)). Thus, the system with the original parameter set did not effectively model those strains. The new parameter set gives better agreement between the DFT calculations and the bond-valence potential model (Figure 6(b)). To solve the problem in the previous potential parameters, we added more reference structures with a variety of lattice constants. The tetragonal-to-cubic phase transition temperature from the new parameter set is ≈700K, which is much closer to the experimental value than the old parameters in Reference 39.

While $PbTiO_3$ has been believed to be a typical displacive ferroelectric, some experimental evidence reveals an order-disorder behavior in this material.[42–44] The evidence suggests that the Pb ions are disordered over 6 sites along the cubic principal axes. Unfortunately, despite the evidence that supports the notion of an order-disorder behavior in $PbTiO_3$, there is difficulty in interpreting experimental results. Using the improved potential parameters, we studied the displacive and order-disorder character of $PbTiO_3$.

Below the phase transition temperature, three clearly separated peaks are observed for both Ti-O and Pb-O bonds. The histogram of Ti-O bond lengths shows three peaks: a peak centered at 1.8Å with the area of S, a peak centered at 2.4Å with the area of S, and a peak centered at 2.0Å with the area of 4S. The histogram of Pb-O bond lengths will show three peaks with the same areas of 4S: a peak centered at 2.5Å, a peak centered at 3.3Å, and a peak centered at 2.8Å. When the histogram of the Ti displacement below T_c is compared with the histogram above T_c, the order-disorder character of $PbTiO_3$ becomes clear. Below T_c, the distribution of each ion has a single peak with the same sign of displacements. If $PbTiO_3$ had only the displacive character, the displacement distribution above T_c should be a single peak. The distribution of the Ti displacement has symmetric double peaks, which confirms that there is an order-disorder

characteristic for $PbTiO_3$ in the paraelectric phase. The same behavior was shown for the Pb displacement.

4. Conclusion

Using first-principles DFT calculations, we have investigated the properties of solid oxide materials. We have been able to probe the structural and electronic environment of $Ba(Ce_{1-x}Pd_x)O_{3-\delta}$, which contains both O vacancies and dopants. These stablized impurities give rise to new catalysts with interesting possibilities for future tailored designs. Our study yields insights into how an oxide lattice accomodates impurities, and how use O diffuse through the bulk and to the surface. For bulk relaxor ferroelectrics, relationships between atomic composition, experimentally determined properties and technologically important properties were elucidated. These offer guidance for the design of new piezoelectric materials with superior performance. Our molecular dynamics simulations of the order-disorder character of $PbTiO_3$ have shown that the classical theory of a simple displacive transition is inaccurate. Incorporation of this behavior into our bond valence model has led to improved theoretical properties that are closer to experiment.

The authors would like to thank P.K. Davies, I.W. Chen, S.L. Scott and R. Seshadri for many useful discussions. This work was supported by the Office of Naval Research under grant number N-000014-00-1-0372. We also acknowledge the support of the National Science Foundation, through the MRSEC program, Grant No. DMR0520020 and the Air Force Office for Scientific Research, Grant No. FA9550-07-1-0397. Computational support was provided by the High-Performance Computing Modernization Office of the Department of Defense and the Center for Piezoelectrics by Design. Correspondence and requests for materials should be addressed to A.M.R. (email: rappe@sas.upenn.edu).

5. Significance to DoD

Perovskite oxides are used extensively in modern Naval SONAR (sound navigation and ranging) devices, non-volatile memories, and telecommunications applications. The US Navy would reap a considerable military advantage from developing SONAR-detecting materials, microwave materials, and improved fuel cells with higher performance, lower cost, and less harmful environmental side effects. Understanding the behavior of current perovskite oxides is critical for the goal of developing new materials. Once the relationships between the atomic composition, structure and materials properties are understood, new materials that improve upon existing technology can be designed. Our DFT calculations have revealed the microscopic origin of relaxor behavior which sets the operating range of piezoelectric devices, and suggest a series of new promising compositions for next-generation piezoelectric materials. We have also used DFT to understand how common problems like O vacancies can actually be used with the correct chemical environment to create what could be a better fuel cell. Also, molecular dynamics simulations of polarized materials are vital for obtaining microscopic insight and guidance for design of efficient and robust nonvolatile ferroelectric memory devices, for use in the challenging Navy operating environment. The main method of undersea detection relies on SONAR with ferroelectric materials. The development of the multiscale computational method for these materials will enable the study of the intrinsic properties of ferroelectric domain dynamics to understand the polarization reversal process in the atomistic scale and provide a possible way to increase the sensitivity of SONAR.

Systems Used

The work presented here was performed on the Engineer Research and Development Center's Cray XT3, the Arctic Region Supercomputer Center's Sun Opteron Cluster and the Army High Performance Computing Research Center's Cray X1E machines. With regards to our in-house code, ionic relaxations typically run in about a day on the X1E machine and about a week on the XT3 and Opteron machines. DFT codes use an iterative diagonalization procedure to solve quantum mechanical calculations that rely heavily on BLAS and LAPACK routines. Especially suited to run on the vector Cray X1E is our in-house code, which performs with 90% vector efficiency. This gives rise to an order of magnitude difference in run time between the X1E and XT3 platforms. Typically, runs use 4 to 16 processors, which in the case of the X1E platform are 4 to 16 MSP, where each MSP itself consists of 4 processors. This code is highly scalable with a parallelization efficiency of almost 100% for a small numbers of processors (<20) and dropping off to slightly above 50% at 128 processors. For the PbTiO3 simulations, we used MOLDY (an MD program which was developed by Keith Refson under the GNU General Public License) and VASP (a DFT code developed by G. Kresse). All calculations were performed on Cray XT3 (sapphire). These programs are effectively parallelized with MPI. Since the supercell size of DFT calculations was as small as 1 or 4 unit cells, 4 or 8 nodes were used. MD simulations were usually performed in 32 nodes with a parallelization efficiency of larger than 75 %.

Computational Technology Area

Computational Materials Science

References

1. Hohenberg, P. and W. Kohn, *Phys. Rev.*, 136, B864, 1964.

2. Kohn, W. and L.J. Sham, *Phys. Rev.*, 140, A1133, 1965.

3. Grinberg, I., V.R. Cooper, and A.M. Rappe, *Nature*, 419, 909, 2002.

4. Fu, H. and R.E. Cohen, *Nature*, 402, 281, 2000.

5. George, A.M., J. Iniguez, and L. Bellaiche, *Nature*, 413, 54, 2001.

6. Grinberg, I., P. Juhas, P.K. Davies, and A.M. Rappe, *Phys. Rev. Lett.*, 99, 267603, 2007.

7. Li, J., U.G. Singh, J.W. Bennett, K. Page, J. Weaver, J.P. Zhang, T. Proffen, A.M. Rappe, S. Scott, and R. Seshadri, *Chem. Mater.*, pp. 1418–23, 2007.

8. Singh, U.G., J. Li, J.W. Bennett, A.M. Rappe, R. Seshadri, and S.L. Scott, *J. Catal.*, 249, 347, 2007.

9. Perdew, J.P. and A. Zunger, *Phys. Rev. B*, 23, 5048, 1981.

10. Ramer, N.J. and A. M. Rappe, *Phys. Rev. B*, 59, 12471, 1999.

11. Rappe, A.M., K.M. Rabe, E. Kaxiras, and J.D. Joannopoulos, *Phys. Rev. B Rapid Comm.*, 41, 1227, 1990.

12. Davidson, E.R., *J. Comput. Phys.*, 17, 87, 1975.

13. Bendtsen, C., O.H. Nielsen, and L.B. Hansen, *Appl. Num. Math.*, 37, 189, 2001.

14. Pulay, P., *J. Comp. Chem.*, 3, 556, 1982.

15. Pfrommer, B.G., M. Coté, S.G. Louie, and M.L. Cohen, *J. Comp. Phys.*, 131, 233, 1997.

16. Brown, I.D., *Structure and Bonding in Crystals II*, edited by M. O'Keeffe and A. Navrotsky, Academic Press, New York, NY, 1981, pp. 1–30.

17. Nishihata, Y., J. Mizuki, T. Akao, H. Tanaka, M. Uenishi, M. Kimura, T. Okamoto, and N. Hamada, *Nature*,418, 164, 2002.

18. Tanaka, H., M. Taniguchi, M. Uenishi, N. Kajita, I. Tan, Y. Nishihata, J. Mizuki, K. Narita, M. Kimura, and K. Kaneko, *Angew. Chem. Int. Ed*, 45, 5998, 2006.

19. Proffen, T. and S.L. Billinge, *J. Appl. Cryst.*, 32, 572, 1999.

20. Grinberg, I., V.R. Cooper, and A.M. Rappe, *Phys. Rev. B*, 69, 144118, 2004.

21. Juhas, P., I. Grinberg, A.M. Rappe, W. Dmowski, T. Egami, and P.K. Davies, *Phys. Rev. B*, 69, 214101, 2004.

22. Grinberg, I. and A.M. Rappe, *Phys. Rev. B*, 70, 220101, 2004, ISSN 0163-1829, URL: http://dx.doi.org/10. 1103/ PhysRevB.70.220101.

23. Grinberg, I., M.R. Suchomel, P.K. Davies, and A.M. Rappe, *J. Appl. Phys.*, 98, 094111, 2005.

24. Cohen, R.E., *Nature*, 358, 136, 1992.

25. Burton, B.P. and E. Cockayne, *Phys. Rev. B Rapid Comm.*, 60, 12542, 1999.

26. Fisch, R., *Phys. Rev. B*, 67, 094110, 2003.

27. Farber, L. and P. Davies, *J. Am. Ceram. Soc.*, 86, 1861, 2003.

28. Akbas, M.A. and P.K. Davies, *International Journal of Inorganic Material*s, 3, 123, 2001.

29. Akbas, M.A. and P.K. Davies, *J. Am. Ceram. Soc.*, 80, 2933, 1997.

30. Kumar, A., K. Prasad, S. Choudhary, and R. Choudhary, *Mater. Lett.*, 58, 3395, 2004.

31. Bing, Y-H., A. Bokov, Z-G. Ye, B. Noheda, and G. Shirane, *J. Phys: Cond. Matt*., 17, 2493, 2005.

32. Dawber, M., K.M. Rabe, and J.F. Scott, *Rev. Mod. Phys.*, 77, 1083, 2005.

33. Merz, W.J., *Phys. Rev.*, 95, 690, 1954.

34. Miller, R.C. and G. Weinreich, *Phys. Rev.*,117, 1460, 1960.

35. Stadler, H.L. and P.J. Zachmanidis, *J. Appl. Phys.*, 34, 3255, 1963.

36. Tybell, T., P. Paruch, T. Giamarchi, and J.-M. Triscone, *Phys. Rev. Lett.*, 89, 097601, 2002.

37. Gruverman, A., B.J. Rodriguez, C. Dehoff, J.D. Waldrep, A.I. Kingon, R.J. Nemanich, and J.S. Cross, *Appl. Phys. Lett.*, 87, 082902, 2005.

38. Grigoriev, A., D.H. Do, D.M. Kim, C.B. Eom, B. Adams, E.M. Dufresne, and P.G. Evans, *Phys. Rev. Lett.*, 96, 187601, 2006.

39. Shin, Y-H., V.R. Cooper, I. Grinberg, and A.M. Rappe, *Phys. Rev. B*, 71, 054104, 2005, ISSN 0163-1829, URL: http://dx.doi.org/10.1103/PhysRevB.71.054104.

40. Shin, Y-H., I. Grinberg, I-W. Chen, and A.M. Rappe, *Nature*, 449, 881, 2007.

41. Shin, Y-H., B-J. Lee, and A.M. Rappe, *J. Korean Phys. Soc.*, 52, 1206, 2008, ISSN 0374-4884.

42. Fontana, M.D., H. Idrissi, G.E. Kugel, and K. Wojcik, *Journal of Physics: Condensed Matter*, 3, 8695, 1991, URL: http://stacks.iop.org/0953-8984/3/8695.

43. Nelmes, R.J., R.O. Piltz, W.F. Kuhs, Z. Tun, and R. Restori, *Ferroelectrics*, 108, 165, 1990.

44. Kiat, J-M., Y. Uesu, B. Dkhil, M. Matsuda, C. Malibert, and G. Calvarin1, *Phys. Rev. B*, 65, 064106, 2002.

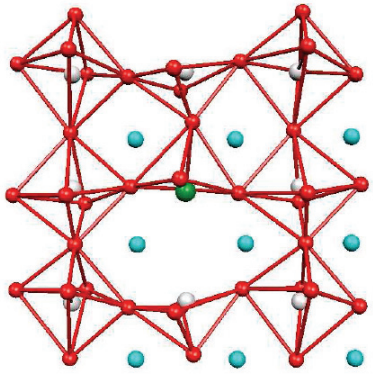

Figure 1. $Ba(Ce_{1-\delta}Pd_{\delta})O_{3-\delta}$ Structure 1, where Pd dopant is adjacent to an O vacancy. This shows lesser degree of octahedral distortion of the nearest neighbors than Structure 2, as well as more symmetric tilts. Pd is green, Ba are light blue, Ce are gray and O red.

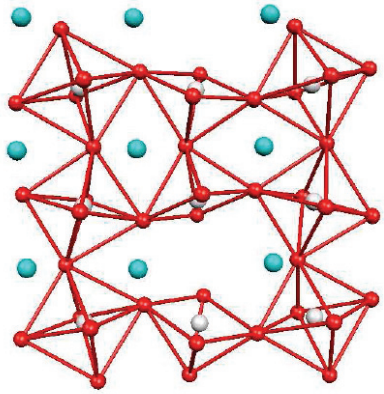

Figure 2. $Ba(Ce_{1-\delta}Pd_{\delta})O_{3-\delta}$ Structure 2 has an O vacancy between two Ce atoms, not adjacent to Pd (lower plane, not shown). Ba are light blue, Ce are gray and O red.

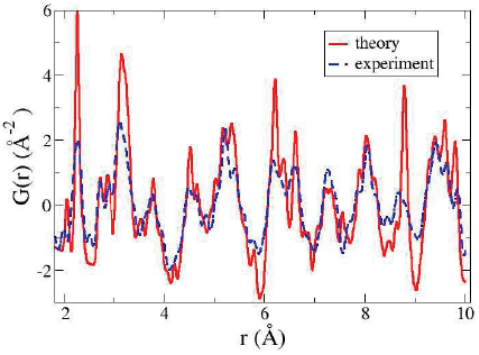

Figure 3. Experimental neutron PDF $G(r)$ of BCP, shown in dashed blue line, and DFT PDF $G(r)$ of Structure 1, shown in solid red line. Experimental BCP was of formula $Ba(Ce_{1-x}Pd_x)O_{3-\delta}$ where x=0.10.

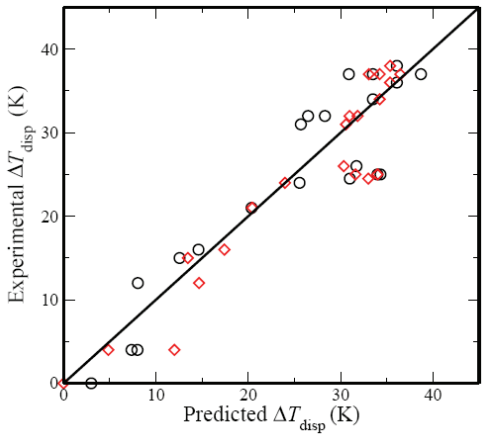

Figure 4. Comparison of local structure model prediction of ΔT_{disp} with experimental values for 21 B-site ordered relaxor material compositions. Linear model (circles) and Landau theory model (diamonds) provide good agreement with experiment yielding average ΔT_{disp} errors of 3.7K and 2.9K respectively.

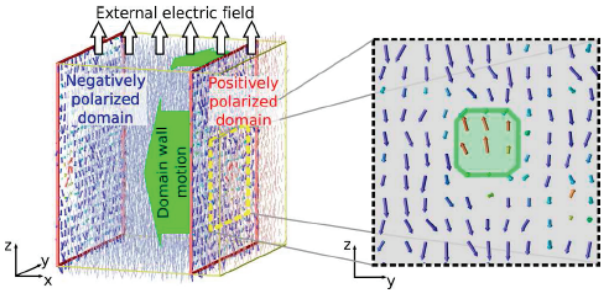

Figure 5. A snapshot of the polarization from a molecular dynamics simulation of $PbTiO_3$. Each arrow denotes the local polarization of a unit cell. This simulation reveals that thecritical nucleus is much smaller than previously thought (3 × 3 cells or 12 Å × 12 Å). This explains recent reports of rapid ferroelectric domain wall motion.

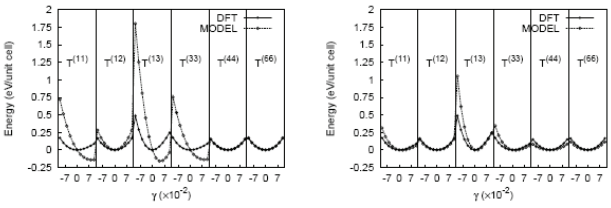

Figure 6. Improved bond valence modeling of $PbTiO_3$ under strain. Comparison between the DFT calculation and the model potential with (a) the potential parameters in Reference 39 and (b) the potential parameters in this study.